

# CFD SIMULATION OF NATURAL CONVECTION COOLING AFTER A LOSS-OF-FLOW TRANSIENT

**A. Kraus and R. Hu**

Nuclear Engineering Division  
Argonne National Laboratory  
9700 S Cass Ave., Argonne, IL, 60439, USA  
akraus@anl.gov; rhu@anl.gov

## ABSTRACT

Natural convection cooling is of ever-increasing importance in nuclear reactor safety, particularly for long transients. One relevant accident scenario is the Protected Loss-of-Flow (PLOF) transient, which relies on natural convection cooling for decay heat removal in many pool-type and integral-vessel reactors. A reference design investigated here is the Prototype Gen-IV Sodium Fast Reactor (PGSFR), a pool-type design with 150 MWe output power. Whole-vessel steady-state Computational Fluid Dynamics (CFD) simulations of a reference PGSFR design were performed in STAR-CCM+ to assess the long-term cooling capability of the Decay Heat Removal Heat Exchangers (DHXs) for a PLOF scenario. A porous media approach was employed for a number of internal structures to make the problem tenable. It was found that a segregated flow method with an additional dissipation term for pressure yielded results comparable to those of the recommended coupled flow solver, but with greater solver robustness and faster convergence. CFD results were compared with 1-D SAS4A/SASSYS-1 system code simulations, which showed reasonable agreement. These simulations provide evidence that placement of the DHXs in the cold pool is appropriate, and that effective long-term cooling of the core decay heat could be feasibly achieved for the PLOF transient.

## KEYWORDS

natural convection, loss of flow, sodium-cooled fast reactor, porous media, computational fluid dynamics

## 1. INTRODUCTION

Reliable, long-term cooling of nuclear reactor decay heat has been a key thermal-hydraulic challenge for decades. In recent years, particularly in light of the Fukushima disaster, much research has focused on natural convection cooling, with long effective cooling times, fewer active/powered components and a reduced chance of failure. A number of proposed pool-type and integral-vessel reactor designs rely extensively on natural convection cooling in accident scenarios.

There are a number of challenges in simulating and designing a natural convection flow system. First, the heat and flow fields are more strongly coupled than in forced flow, and can require different simulation methods. This means that the entire flow-path between the heat source and sink must be modeled to effectively describe the flow behavior. In a nuclear reactor system, this is generally a large domain filled with complex geometry. Natural convection systems are also inherently unsteady and can frequently have three-dimensional aspects. Uncertainties in loss coefficients and other system parameters may be larger for low-flow conditions. For all of these reasons, significant approximations must typically be made in analyses of these types of systems.

One of the most important transients typically involving natural convection cooling is the Protected Loss-of-Flow (PLOF) transient, in which SCRAM is successful but pumps coast down and forced flow is lost. This is one example of a “station blackout” event, in which offsite power may be unavailable for a long period. In pool-type reactors, decay heat is typically removed through Decay Heat Removal Heat Exchangers (DHXs) placed into one of the pools.

A reference design analyzed here is the Prototype Gen-IV Sodium Fast Reactor (PGSFR) [1-3], currently being developed by the Korea Atomic Energy Research Institute (KAERI) and Argonne National Laboratory (ANL). This fast-spectrum burner reactor is planned to transmute transuranics (TRU) and produce power as part of an advanced fuel cycle. This is a small modular reactor (SMR), with 150 MWe power output and a pool-type primary system configuration. It should be noted that the design used in this analysis is not the current PGSFR design, but an older design version used during its development. While the natural convection analysis is performed for one specific reactor design, it is intended that the methods applied here can be used in similar transients for other reactor types. This includes other pool-type reactors, notably other SFRs, but also includes single-phase transients in integral-vessel LWRs and other SMR designs.

Natural convection heat removal has been explored for a number of different reactor applications. Parthasarathy et al. [4] used computational fluid dynamics (CFD) with a coarse mesh to investigate steady-state and transient natural convection. However, their DHXs were placed in the hot pool, while it is planned to place the PGSFR DHXs in the cold pool. For the PGSFR design, it was shown [5] that the hot-pool placement led to scenarios in which the hot pool could be overcooled to have a temperature lower than that of the cold pool. This could lead to stagnation or flow reversal in some areas of the core, which is undesirable. The difference in placement will greatly change flow patterns and somewhat limits the analogy that can be made between the two systems. Hung et al. [6] investigated detailed physical modeling parametrics of the vessel cooling of an SFR, but these were largely limited to 2D CFD calculations with 1<sup>st</sup>-order convection. Abanades and Pena [7] and Vanderhaegen et al. [8] investigated cooling for lead-bismuth eutectic systems, but had similar simplifications to those found in [6]. It should also be noted that since natural convection flow is driven largely by thermal center heights and frictional resistances, care should be taken in generalizing behavior from that of another reactor design.

CFD simulations were performed to assess the natural convection cooling capability of the PGSFR design. Based on the above discussion, to the authors’ knowledge, this study is one of the first 3-D, whole-vessel natural convection CFD simulations of a pool-type reactor, particularly with cold-pool DHX placement. The steady-state simulation of the long-term core cooling after a PLOF transient was investigated, to confirm cold-pool DHX placement could provide sufficient long-term cooling in an accident scenario. In the current scenario, two of the four DHXs are assumed to fail, and the other two DHXs (off-diagonal) are assumed to remove their full capacity of 2MW of heat from the system. This corresponds to 0.5% of full power, occurring roughly 24 hours after the start of the transient. Given the indefinite design of many components and uncertainties used in many of the modeling parameters, the main purpose of the simulation is to gain insight into flow patterns, obtain reasonable estimates of temperatures and flow rates, and to establish whether the current geometry is feasible for long-term natural circulation cooling of the reactor.

The basic PGSFR system layout and natural circulation flow path are provided in Fig. 1. Cold sodium enters the core from the cold pool, is heated, and is ejected to the hot pool, some of which passes through the Upper Internal Structure (UIS). It then flows through Intermediate Heat Exchangers (IHXs) to the cold pool, where it is circulated to the DHXs. The primary flow is cooled and then exits the DHX and enters the pump to be circulated to the core inlet again, completing the loop. The DHXs are sodium-to-sodium heat exchangers, which are linked to another sodium-to-air heat exchanger that links the system to the colder environmental air temperature and drives the flow.

The CFD simulations were compared with results from the 1-D code SAS4A/SASSYS-1 (“SAS”) [9]. The full 3-D modeling in CFD should be able to better capture the details of the flow patterns as well as the expected flow stratification. These CFD results can be used to improve the hot pool and cold pool modeling in SAS. Thus the 1-D code could be used for future transients, reducing the need for more computationally-intensive CFD simulations.

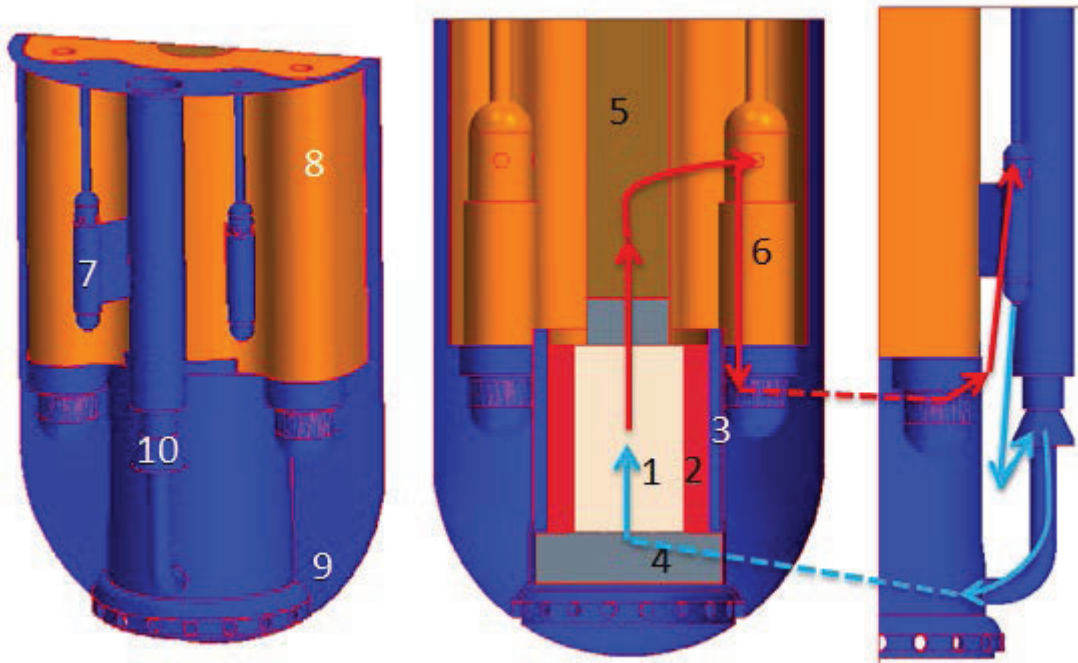


**Figure 1. PGSFR system layout (outer vessel wall removed), showing the core (1), reflector (2), storage ring (3), inlet plenum (4), UIS (5), IHXs (6), DHXs (7), hot pool (8), cold pool (9), and pumps (10). Natural convection flowpath is denoted by the arrows. Center and Right view are orthogonal.**

## 2. METHODS

Since the CFD simulation of a long reactor transient is generally still impractical, Reynolds-Averaged Navier-Stokes (RANS) steady-state simulations of natural circulation flow and heat transfer have been conducted using the commercial CFD code STAR-CCM+ [10]. Instead of simulating the whole PLOF transient, the reactor core decay heat power is fixed at 2 MW, and only the two active DHXs remove heat from the cold pool. Since these decay heat conditions correspond to roughly 24 hours into the transient, pumps are assumed to have fully coasted down.

STAR-CCM+ is a finite volume formulation code, used here for the analysis of incompressible flow and heat transfer. It supports the use of unstructured polyhedral mesh elements, greatly simplifying the generation of computational meshes for complex geometries. The computational mesh was constructed based on CAD data describing the PGSFR geometry. The surfaces were prepared and the system was meshed with polyhedral cells as shown in Fig. 2. A prismatic wall layer was used for more accurate turbulence modeling, with  $30 < y^+ < 300$  for all walls. The final mesh consists of 2.9 million polyhedral and prismatic polygonal cells.

Simplifications are required to generate a moderate CFD model of the complete primary sodium coolant loop, which can be run on a moderate cluster within moderate time. The fuel assemblies, upper internal structures, tubes and support plates in IHXs and DHXs are modeled through a porous media approach. In this approach, the macroscopic effect of the porous region is taken into account as a source term in the momentum equation. Thus the detailed geometry of these regions is not modeled. For the final CFD model, the cold pool, hot pool, core inlet plenum, pump lines, and IHXs are modeled as pure fluid regions; the rest are treated as porous media.

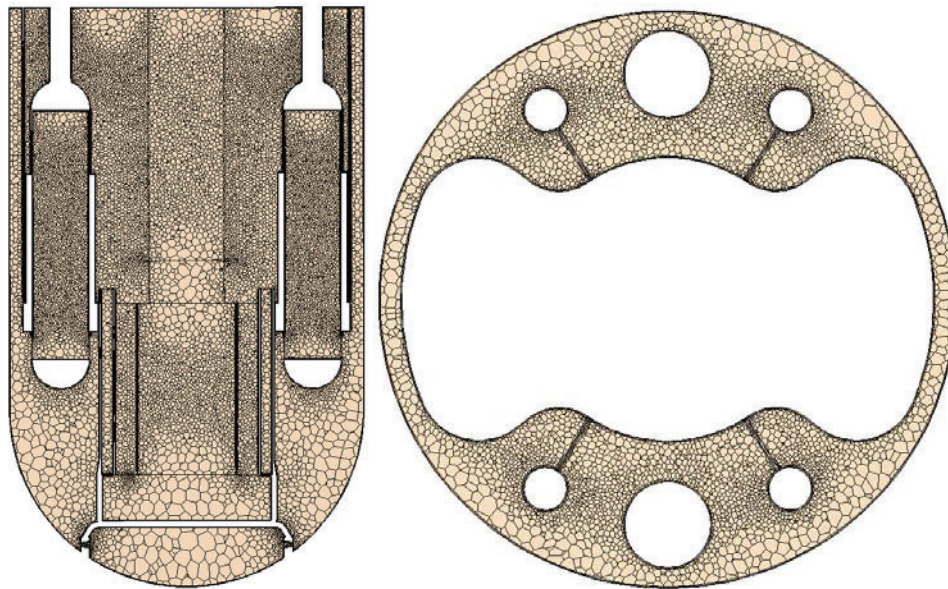


**Figure 2. Mesh Distribution in the Base Model**  
(left: cut view of IHX cross-plane; right: top view of a cold pool horizontal cross-plane).

## 2.1. Porous Media Parameter Development

The two general forms for pressure drop in porous media are given in STAR-CCM+ as

$$\frac{dP}{dz} = -(\alpha|v| + \beta) \cdot v \quad (1)$$

$$\Delta P = -\rho(\alpha|v_n| + \beta)v_n \quad (2)$$

The first equation corresponds to a full porous region, while the second equation is for porous baffles. Here  $v$  is the fluid velocity vector and  $\alpha$  and  $\beta$  are tensors, termed the inertial and viscous loss coefficients, respectively. The resistance coefficients were derived based on a number of data sources or empirical correlations, and are summarized in the following sections. Simple stand-alone CFD models were constructed for each individual component to confirm that the coefficients produced the desired pressure drop for the geometry.

### 2.1.1. Core channels

Pressure drop data for the different core assemblies were obtained from runs previously performed using the SUPERENERGY-2 subchannel code [11]. These runs were performed at both nominal and reduced flow rates with realistic orificing [12]. Since the flow volume is significantly larger in the porous model

than the actual geometry, an area scaling was performed to achieve the same pressure drop for the same flow rate. A polynomial fitting was applied to the data points, as shown in Fig. 3. Only reduced flow data were utilized, which provided 24 data points and resulted in a better fit in the low-flow range. This is appropriate for the flow rates expected during the natural circulation cooling.

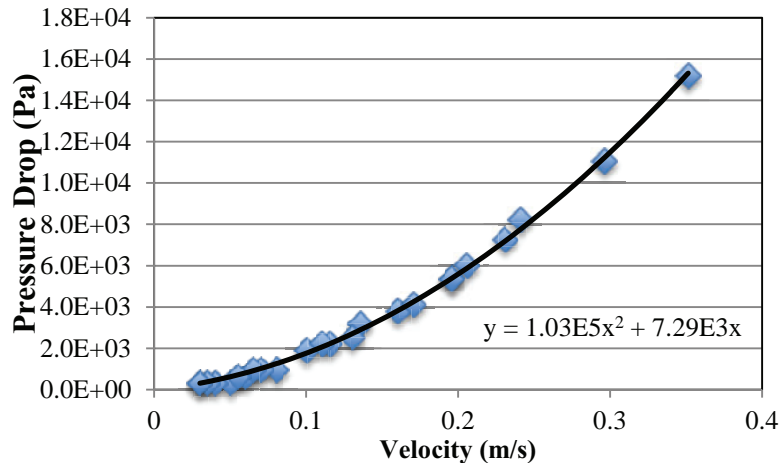


**Figure 3. Pressure Drop vs. Velocity Curve for the Core Channel Region.**

### 2.1.2. Reflector/shield and storage ring

The reflector/shield region porous loss coefficients were also derived from the SUPERENERGY-2 simulations. However, there were only five total data points, and all were above the nominal flow rates. Thus, there is higher uncertainty in the derived coefficients. The storage ring is filled with an undetermined number of spent fuel assemblies, surrounding the core barrel. In order to prevent swirling and unrealistic flow patterns from developing, a uniform resistance equal to that of the core region was used to simulate resistance due to the stored assemblies. Radial heat conduction and the heat generation in the region are neglected in these areas, so there should be little buoyancy head there. Little flow is expected for these regions. Inlet orifice regions were modeled as porous baffles. The resistances were averaged from channel orifice coefficients computed by SAS calculations. Only the coefficient  $\alpha$  for the inertial pressure drop is considered for the baffles.

### 2.1.3. DHXs and IHXs

The DHX and IHX regions contain notable multi-dimensional flow on the primary side since the inlet flow is horizontal while the outlet flow is vertical. Given lack of design data, it was assumed that these directional components had equal resistances. The design pressure drop and flow rate were taken from a 0-D lumped parameter approach and provided only one data point [13]. A linear fit was performed using the data point and the zero-flow, zero-pressure-drop condition. Only a viscous loss coefficient was used given the single data point. The uncertainty of these parameters is expected to be large. The IHX data point was at nominal flow, much higher than the expected flow during natural circulation. However, using even zero porous resistance in the stand-alone CFD analysis for the IHXs provided a drop nearly equal to the design data. For this and other reasons explained later, the approach for the IHXs was changed from a porous to a regular fluid region. In future cases, as IHX design data is finalized, generating the porous coefficients may be revisited.

#### 2.1.4. UIS

Details of the UIS region were still under development at this stage of the design process. However, the region is expected to provide a non-negligible flow resistance and should be modeled. The only portion of the available UIS design information is the control rod locations. Resistance coefficients were approximated using correlations for rod lattices, with pitch and diameter values estimated from the control rod drive placements.

The control rods were approximated as being similar to a triangular array with a P/D ratio of about 3. For the axial resistance, the friction factor was obtained from a polynomial fit by Todreas and Cheng to data obtained by Rehme [14]. For flow laterally across the control rods, the Zukauskas correlation was employed [14]. The top portion of the UIS features a cylindrical outer surface with circular holes to allow sodium to pass through. For simplicity, the resistance through this surface was estimated as a sharp edge.

The current UIS resistance values are certainly underestimated. In reality, the UIS will contain other structures such as instrumentation, but the effects of these structures are difficult to estimate. It is important to note that although there are very large uncertainties in the data used in these correlations, the derived porous resistance values are very small: roughly one order of magnitude less than the DHX and several orders of magnitude lower than the core region. Moreover, flow can bypass the UIS, unlike other key components such as the core and IHXs. This should minimize the effect of the uncertainty in UIS resistance coefficients on the global flow behavior in the full system CFD simulation.

Table I provides a list of the porous resistance coefficients for all porous regions in the CFD model. The core and reflector/shield regions, including the orifice, have the dominant resistance by a large margin to natural convection flow. Since these regions have the most data points for verification, the overall pressure drop for the model should be fairly well established. This also means that the effect of the uncertainties in establishing resistances for the other regions should be relatively minor. For future work, it is important to obtain a more confident pressure drop estimate and design data for the DHX region in particular. The local pressure drop in the DHX affects the primary flow rate there and hence the outlet DHX temperature, which affects the buoyancy source and the flow pattern in the cold pool.

**Table I. Resistance Coefficients for All Porous Regions  
(for tensor  $\alpha$  and  $\beta$ , value given is along the primary flow direction unless otherwise stated)**

Region	$\alpha$ (kg/m <sup>4</sup> , unitless for orifices)	$\beta$ (kg/m <sup>3</sup> /s, m <sup>-1</sup> for orifices)
Core Channels	103332	7289.26
Core Inlet Orifice	35788	0
Reflector/Shield Channels	762326	146395
Reflector/Shield Inlet Orifice	$1.2415 \times 10^8$	0
Storage Ring	103332	7289.26
DHX	0	5600
IHX	0	0
UIS Internal (axial)	21.731	0
UIS Internal (lateral)	290.67	0
UIS Outer Cylinder	418.058	0

## 2.2. Physical and Numerical Modeling Description

In the CFD analysis of the PGSFR long-term decay heat removal performance, the flow in the primary coolant system is treated to be a steady 3D, turbulent, incompressible flow. Sodium is the working fluid with constant material properties except the density, which is dependent on a polynomial correlation, the same used in SAS [9]. No flow boundary conditions were specified for the primary coolant system since the whole system is under natural circulation. All walls are treated as adiabatic, no-slip walls. Thus conduction is not modeled between the hot and cold pools. However, in reality the presence of pool-to-pool conduction should only serve to improve the stratification in the cold pool, improving heat removal capability of the DHX.

Turbulence was modeled using the Realizable  $k$ - $\epsilon$  model with a buoyancy-driven two-layer wall model formulation [15-16]. A uniform power density corresponding to 2MW of power is assumed in the core region. All convective terms were discretized using a second-order upwind formulation.

The dual-stream heat exchanger model in STAR-CCM+ is applied to the two active DHXs, for which the secondary side flow is also modeled with a porous approach. Constant secondary side inlet flow and temperature conditions were provided [13]. The secondary side global heat transfer coefficient was specified such that total heat removal was 2 MW. Thus it must be stressed that the results from these simulations attempt to show what the flow and temperature fields should be if the system were indeed to operate at its 2 MW capacity.

In general, the Coupled Flow and Coupled Energy Models in STAR-CCM+ are recommended for natural convection problems and flows with large body forces or energy sources [10]. However, convergence was found to be very slow using the coupled solvers for the simulation of the PGSFR primary coolant system. This is because this approach solves the system as a pseudo-transient, and for this natural circulation case the flow velocity is small and the system is large.

The Segregated Flow Model solves the flow equations (one for each component of velocity, and one for pressure) in a segregated, or uncoupled, manner through use of the SIMPLE algorithm. Although this model has its roots in constant-density flows, it is capable of handling low Rayleigh number natural convection [17]. This approach also uses the Segregated Energy Model, which solves the temperature field after the flow field is obtained by the segregated flow solver. This method is often faster and uses less memory than the coupled algorithm.

The default segregated solver can have issues solving the flow for domains with porous regions, notably at the interfaces between porous and non-porous regions. Early investigations of the PLOF using the standard segregated solver were very unstable. STAR-CCM+ provides one method for improving robustness for these problems. This is accomplished by adding a “Delta-V” dissipation term to the pressure evaluation. In this case, the cell face pressure,  $p_f$ , is evaluated as

$$p_f = \frac{\bar{a}_0 p_{f0} + \bar{a}_1 p_{f1}}{\bar{a}_0 + \bar{a}_1} + \frac{2\bar{a}_0 \bar{a}_1}{\bar{a}_0 + \bar{a}_1} \cdot \frac{(\mathbf{v}_{f0} - \mathbf{v}_{f1}) \cdot \mathbf{a}}{4(\mathbf{a} \cdot \mathbf{a})} \quad (3)$$

where  $\bar{a}$  is the average momentum coefficient,  $\mathbf{v}$  is the reconstructed face velocity, and  $\mathbf{a}$  is the face area vector. Subscripts “0” and “1” refer to two adjacent cells. The first term of (3) is the standard evaluation and the second term is the added Delta-V dissipation term [10]. This term essentially makes the segregated solver behave more like the coupled solver by more directly linking the pressure and velocity

fields. Results from this modified segregated method were similar to those from the coupled method, but displayed faster and more robust convergence behavior.

Struggles with turbulence convergence were part of the reason for modeling the IHX as a fluid region. STAR-CCM+ does not model turbulence in the porous regions; it instead employs user-specified values for turbulence parameters in the region [10], which affects the turbulence downstream of the porous medium. This can cause convergence issues, particularly if flow reversal occurs during the solution process. Thus, modeling the IHX as a fluid region allowed for explicit turbulence modeling and provided much smoother convergence for the turbulence solver, without sacrificing any significant portion of the pressure drop (see Section 2.1.3).

### 3. SIMULATION RESULTS AND DISCUSSION

#### 3.1. Base Case

Given the slow-developing buoyancy source and low under-relaxation factors necessary for stability, a large number of iterations were required to obtain a converged solution. Residuals for natural convection simulations in particular are not fully indicative of system convergence. Surface-averaged temperatures and flow rates were used in the interested areas to further assess the solution behavior. Fig. 4 shows the residuals of the base case simulation. They decreased very quickly to levels normally associated with a converged solution ( $\sim 10^{-4}$  or lower). However, some macroscopic parameters, notably temperatures, require far more iterations to convergence than the residuals would suggest. Fig. 5 shows the mass flow entering the core and the core outlet temperature. The mass flow rates approach steady values early in the simulation. Fig. 6 demonstrates, however, that the amount of heat removed from the domain by the heat exchanger model is initially higher than the core power, and slowly decreases to the appropriate value (2 MW for this case). This in turn causes the temperatures to take more than 20,000 iterations to converge.

Fig. 7 shows the temperature distribution at different 2-D cross planes of the system domain. The DHX secondary side displays a rather uniform temperature gradient with expected inlet/outlet values. Temperature distributions at other cross planes demonstrated the strong thermal stratification in the cold pool and at the IHX outlet. The large temperature difference and relatively low flow velocity at the IHX outlets leads to a very strong stratification there. There is a strong plume exiting the DHX that also contributes to the stratification. The cold pool top and bottom temperatures are both quite uniform throughout their respective areas, and the hot pool temperature is also very uniform. Strong temperature gradients were observed in the core and reflector/shield regions.

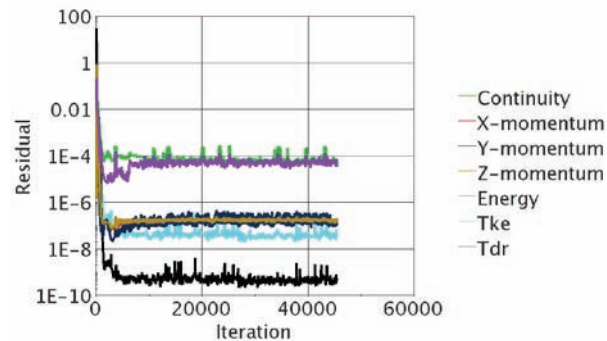
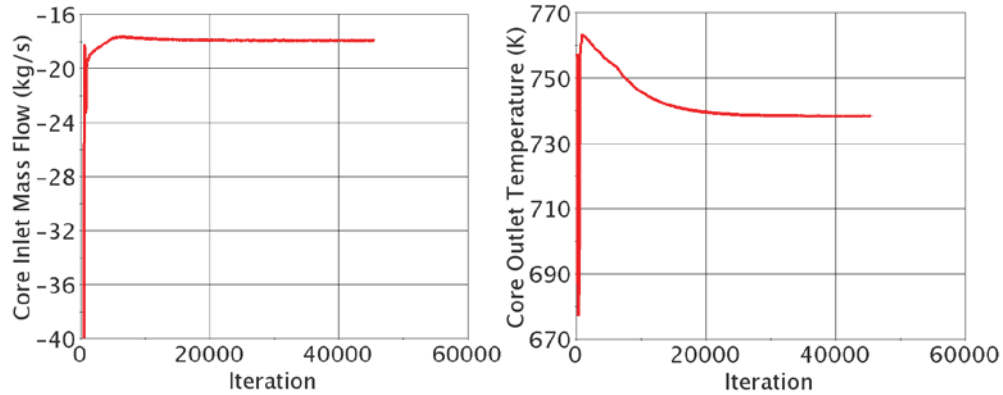
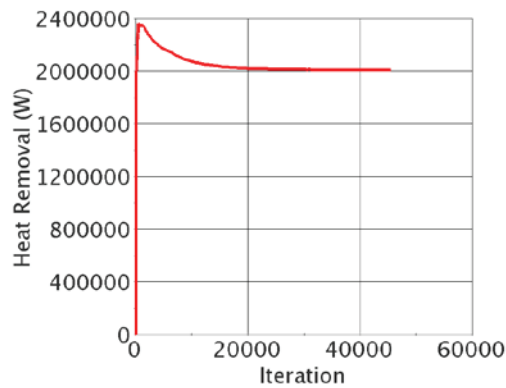


Figure 4. Simulation Residuals.



**Figure 5. Core Inlet Mass Flow (L) and Core Outlet Temperature (R).**



**Figure 6. Heat removed by the DHX Heat Exchanger.**

Fig. 8 provides velocity vector plots along the same cross-planes through the domain. It should be noted that since there are only two operating DHXs, the velocity distribution should not be expected to be symmetric across the pump and IHX planes in these figures. There is again a clear, relatively fast (~0.5 m/s peak) plume emerging from the DHX outlet. The pump velocity vectors are largely symmetric, and the inlet plenum is roughly symmetric in the pump view plane but shows strong recirculation. There is very little flow in the reflector/shield and storage ring areas, as expected from the large porous resistances in those regions. The IHX outlet velocity is strongly influenced by the stratification behavior of the system. Flow in the bottom portion of the outlet region is largely stagnant and significantly colder than the upper portion of the IHX outlet. For this reason the outlet discharge immediately bends to the side and upward at a reasonably high velocity due to buoyancy effects.

### 3.2. Laminar Case

A laminar flow model case was tested to examine the effects of the turbulence model used in the base model. The simulation with laminar flow model was started from the completed base case run to provide good initial conditions. No significant stability issues were encountered. No major deviation from the base case was observed. The plume from the DHX exit extended slightly further into the lower part of the cold pool, but no other global-scale deviations were detected. Table II presents a comparison of results between the two cases. All values are very close to those from the base case. This suggests that, since default (and very uncertain) values were used for all turbulence parameters exiting porous regions, the specific values of these turbulence parameters do not have significant influence on the simulated flow

path and integrated transport quantities. This also means that turbulence is not crucial to obtain the bulk flow properties and behavior that are of interest in this simulation. While laminar cases run faster, the dissipation provided by the turbulence in the base case is helpful from a numerical stability standpoint.

### 3.3. Fine Mesh Case

In order to establish sensitivity to mesh size, a case was also run with a finer mesh throughout the simulation domain. This finer mesh model has around 4.4 million cells, or about 1.5 times as many as the base case, with notable refinement in the cold pool. It was found that the refinement of the mesh caused marginal changes in some of the magnitudes of various solution parameters, but the overall system behavior remained the same and the current design appears feasible for long-term cooling of the reactor. Thus the base mesh was deemed suitable for the main purposes of this analysis.

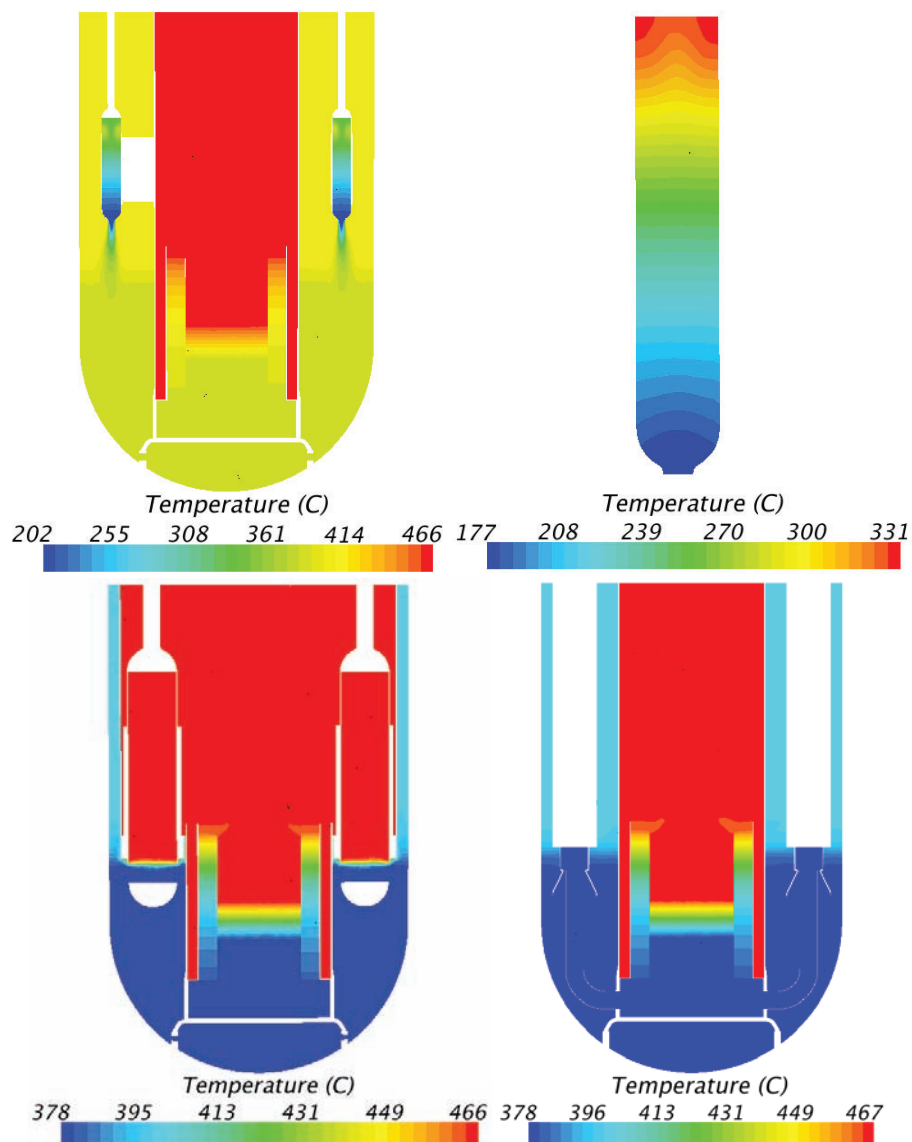
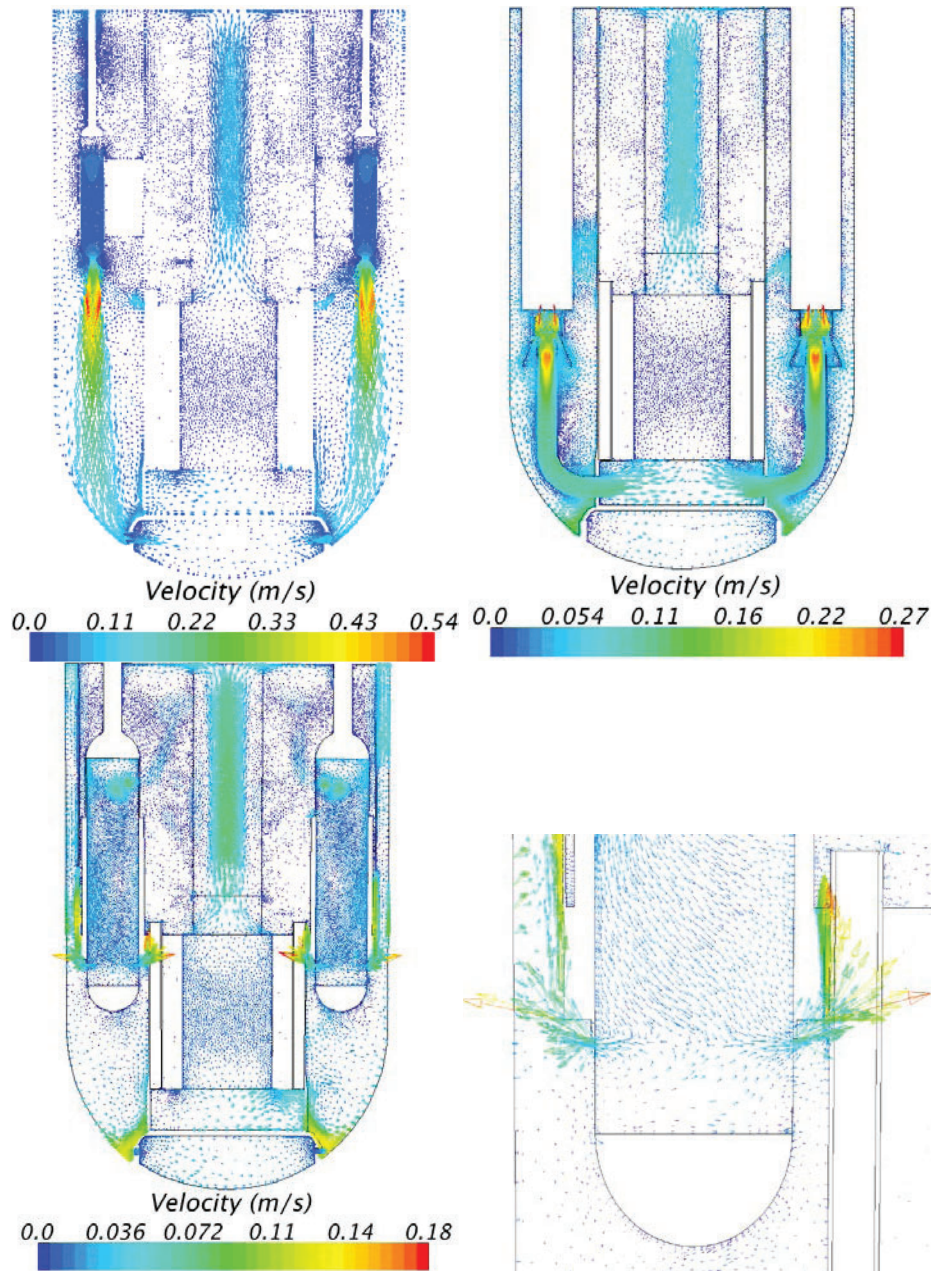


Figure 7. Temperature Distributions, Clockwise from Top Left: DHX View, DHX Secondary Side, Pump View, IHX View.



**Figure 8. Velocity Vector Plots, Clockwise from Top Left: DHX View, Pump View, IHX View, Close-View of IHX Outlet.**

Table III lists major parameters from the base mesh and fine mesh simulation results, as well as the reference SAS results for comparison. Most of the parameters are similar, and close to the SAS results. The stratification is better defined and modeled with the refined mesh, which leads to about 8 degrees lower temperature predictions at the lower part of the cold pool and the hot pool compared to the base case. Many of the results match well between CFD and SAS, notably the DHX primary inlet temperature and secondary outlet temperatures, cold pool top temperature, and core and IHX mass flows. The DHX primary flow rate is reasonably close, but the hot pool, pump intake, and DHX primary outlet temperatures are all roughly 20 °C lower in the CFD results.

**Table II. Comparison of CFD Base Case with Laminar Case Results**

Macroscopic Parameters	Base Case	Laminar Case
Core mass flow (kg/s)	17.9	17.8
Hot pool top temperature (°C)	465	465
Cold pool top temperature (°C)	400	400
Pump intake temperature (°C)	378	378
DHX primary mass flow (kg/s)	4.0	4.0
DHX primary inlet temperature (°C)	400	400
DHX primary outlet temperature (°C)	205	208

**Table III. Comparison between CFD Base Case, Finer Mesh Case, and the Reference SAS Results**

Macroscopic Parameters	CFD Base Mesh	CFD Finer Mesh	SAS
Core mass flow (kg/s)	17.9	17.9	18.6
IHX mass flow (kg/s)	4.55	4.53	4.65
Hot pool top temperature (C)	465	457	483
Cold pool top temperature (C)	400	399	399
Pump intake temperature (C)	378	370	399
DHX primary mass flow (kg/s)	4.0	4.0	4.5
DHX primary inlet temperature (C)	400	399	399
DHX primary outlet temperature (C)	205	204	225
DHX secondary inlet temperature (C)	177	177	177
DHX secondary outlet temperature (C)	329	329	328

The stratification in the cold pool plays a key role in the differences between the CFD results and the SAS calculations. SAS predicted a uniform cold pool temperature that was roughly equal to the CFD predictions in the top part of the cold pool. The core inlet temperature in the CFD simulation is then lower than that in the SAS calculation. The temperature rises through the core are about the same in the two simulations since the predicted core mass flow is similar. The stratification in the cold pool is the key reason why the discrepancies for each of the temperatures between the two codes are nearly the same magnitude. The use of a well-mixed model for the cold pool in the SAS calculation leads to an underestimate of DHX heat removal and overestimate (conservative) of the hot pool temperature.

For the fixed 2 MW heat removal condition, the effectiveness of the DHXs was evaluated through the peak sodium temperatures found in the system. The peak sodium temperature from CFD for the core and hot pool was roughly 467 °C, which is significantly lower than the hot pool temperature of 545 °C for normal operation. This was corroborated by the SAS simulations. These results provide some evidence that the DHX long-term heat removal capability should be sufficient for the PLOF transient.

#### 4. CONCLUSIONS

In summary, steady-state whole-vessel CFD simulations of the PGSFR design during long-term natural circulation cooling have been performed using STAR-CCM+. It can be concluded that a porous media approach is appropriate given the general system behavior of interest and the computational resources available. A modified segregated flow solver was found to have superior convergence behavior as compared to the coupled flow solver for this simulation, and well-converged results were obtained. Results from CFD and a 1-D system code were largely in agreement, but CFD showed a better representation of the flow stratification occurring between the hot and cold pools. This work suggests that the current PGSFR design can provide enough long-term natural circulation cooling of the decay heat in the reactor core after a postulated PLOF transient. The strong thermal stratification observed in the cold pool would enhance the heat removal from the DHX.

The mesh and turbulent vs. laminar model sensitivity studies helped to confirm the above conclusions. Further simulations should be performed for the final design, as well as potentially investigating the effects of pool-to-pool conduction on the system behavior. While the authors believe that the modeling methods used in this work should be applicable to other pool-type and integral-vessel reactors, additional work should be performed to verify the range of problems that can be successfully analyzed with this approach.

#### ACKNOWLEDGMENTS

The authors would like to thank Tyler Sumner and Anton Moissevteyev for performing the SAS4A/SASSYS-1 simulations, Florent Heidet for performing the SUPERENERGY-2 calculations, Prasad Vegendla for CAD cleaning assistance, as well as Mitchell Farmer, Thomas Wei, Christopher Grandy, Yoon Chang, and others for valuable discussions.

This work was funded by Korea Atomic Energy Research Institute under the Work-for-Others Agreement No. 85E20: KAERI-ANL Joint Program on Design Development of a Prototype Sodium-cooled Fast Reactor. The submitted manuscript has been created by UChicago Argonne, LLC, Operator of Argonne National Laboratory (“Argonne”). Argonne, a U.S. Department of Energy Office of Science laboratory, is operated under Contract No. DE-AC02-06CH11357. The U.S. Government retains for itself, and others acting on its behalf, a paid-up nonexclusive, irrevocable worldwide license in said article to reproduce, prepare derivative works, distribute copies to the public, and perform publicly and display publicly, by or on behalf of the Government.

#### REFERENCES

1. D. Hartanto and Y. Kim, “Conceptual Study of a Long-Life Prototype Gen-IV Sodium-Cooled Fast Reactor (PGSFR),” *PHYSOR 2014*, Kyoto, Japan, Sep. 28-Oct. 3, on CD-ROM (2014).
2. A. Shin et al., “Development Status of TRACE Model for PGSFR Safety Evaluation,” *Korean Nuclear Society Spring Meeting*, Jeju, Korea, May 29-30, on CD-ROM (2014).
3. D. Kim, J. Eoh, and T.H. Lee, “An Optimal Design Approach for the Decay Heat Removal System in the PGSFR,” *ASME 4<sup>th</sup> Joint US-European Fluids Engineering Division Summer Meeting (FEDSM)*, Chicago, IL, USA, Aug. 3-7, on CD-ROM (2014).
4. U. Parthasarathy et al., “Decay Heat Removal in Pool Type Fast Reactor Using Passive Systems,” *Nucl. Eng. Des.* **250**, pp. 480-499 (2012).
5. R. Hu et al., Argonne National Laboratory, unpublished information, 2013.
6. T.C. Hung et al., “CFD Modeling and Thermal-Hydraulic Analysis for the Passive Decay Heat Removal of a Sodium-Cooled Fast Reactor,” *Nucl. Eng. Des.* **241**, pp. 425-432 (2011).

7. A. Abanades and A. Pena, "Steady-State Natural Circulation Analysis with Computational Fluid Dynamic Codes of a Liquid Metal-Cooled Accelerator Driven System," *Nucl. Eng. Des.* **239**, pp. 418-424 (2009).
8. M. Vanderhaegen, J. Vierendeels, and B. Arien, "CFD Analysis of the MYRRHA Primary Cooling System," *Nucl. Eng. Des.* **241**, pp. 775-784 (2011).
9. T. H. Fanning, ed., "The SAS4A/SASSYS-1 Safety Analysis Code System," ANL/NE-12/4, Nuclear Engineering Division, Argonne National Laboratory, January 31, 2012.
10. CD-adapco, "STAR-CCM+ 7.02.008 Manual," Melville, N.Y., (2012).
11. K.L. Basehore and N.E. Todreas, "SUPERENERGY-2: A Multiassembly, Steady-State Computer Code for LMFBR Core Thermal-Hydraulic Analysis," PNL-3379, Pacific Northwest Laboratory, August 1980.
12. F. Heidet, Argonne National Laboratory, unpublished information, 2013.
13. M. T. Farmer et al., Argonne National Laboratory, unpublished information, 2013.
14. N. Todreas and M.S. Kazimi, *Nuclear Systems I: Thermal Hydraulic Fundamentals*, Chapter 9, Taylor & Francis, New York, NY, USA (1990).
15. W. Xu, Q. Chen, and F.T.M. Nieuwstadt, "A New Turbulence Model for Near-Wall Natural Convection," *Int. J. Heat Mass Tran.* **41**(21), pp. 3161-3176 (1998).
16. T.-H. Shih, W.W. Liou, A. Shabbir, Z. Yang, and J. Zhu, "A New k- $\epsilon$  Eddy Viscosity Model for High Reynolds Number Turbulent Flows – Model Development and Validation," NASA TM 106721 (1994).
17. S. Patankar and D. Spalding, "A Calculation Procedure for Heat, Mass, and Momentum Transfer in Three-Dimensional Parabolic Flows," *Int. J. Heat Mass Tran.* **15**(10), pp. 1787-1806 (1972).